Optics Letters

Enhancement of surface plasmon polariton excitation via feedback-based wavefront shaping

Xiaona Ye,[1,2] Haigang Liu,[1,2,3] Yanqi Qiao,[1,2] and Xianfeng Chen[1,2,4]

[1]State Key Laboratory of Advanced Optical Communication Systems and Networks, School of Physics and Astronomy, Shanghai Jiao Tong University, Shanghai 200240, China
[2]Key Laboratory for Laser Plasma (Ministry of Education), Collaborative Innovation Center of IFSA (CICIFSA), Shanghai Jiao Tong University, Shanghai 200240, China
[3]e-mail: liuhaigang@sjtu.edu.cn
[4]e-mail: xfchen@sjtu.edu.cn

Received 10 October 2018; revised 13 November 2018; accepted 14 November 2018; posted 15 November 2018 (Doc. ID 347879); published 11 December 2018

Surface plasmon polariton (SPP) is an electromagnetic excitation with efficient spatial confinement and high local field intensity at a metal/dielectric interface, which has been widely applied in many fields such as nanophotonics, imaging, biosensing, nonlinear optics, and so on. However, the destructive interference, which arises from wavevector mismatching between the spatial components of incident light and SPP, limits the effective excitation of SPP. Here, we experimentally demonstrate the enhancement of SPP excitation via a feedback-based wavefront shaping method in the Kreschmann configuration. After optimizing the phase profile of the incident laser beam, the intensity is enhanced by a factor of 1.58 times even at the resonance angle of the fundamental mode Gaussian beam. Besides, the influences of different conditions for the enhancement of SPP excitation are also analyzed. This work provides a flexible and convenient method to further enhance the SPP excitation, and it may have the application of further enhancement of the interaction between SPP and other physical processes.

https://doi.org/10.1364/OL.43.006021

Surface plasmon polaritons (SPPs) are surface electromagnetic waves that tightly bound to metal/dielectric interface, which originate from the strong interaction between an external electromagnetic field and free electron oscillations on the surface of metal [1]. To date, they have been extensively researched in lots of fields due to their unique properties. For instance, SPP excitation is extremely sensitive to the dielectric properties of the surrounding medium, which enable it to be used in highly sensitive biosensing [2]. The coupling of light to SPPs can result in strong local electromagnetic fields, which significantly enhance nonlinear interactions including second-harmonic generation [3], third-harmonic generation [4], four-wave mixing [5], and so on. More interestingly, the spontaneous Raman scattering of molecules can also be enhanced by SPP to improve the detection of weak signals [6,7]. In addition, SPPs can efficiently confine the longitudinal field into the subwavelength scale due to the existence of the evanescent field, which opens up new opportunities for optical trapping at the nanometer-scale [8] and has potential application in the area of on-chip communication and modulation [9].

Given its significant applications in all kinds of areas mentioned above, it is rather important to excite such SPPs efficiently. As we know, effective excitation of SPPs requires that the in-plane wavevector components of the incident photons of free space along the metal/dielectric interface are strictly equal to the SPP wavevector [10]. The common methods of realizing the SPP excitation are by using an optical waveguide coupler [11], diffraction gratings and defects [12], the Otto [13] and Kretschmann configurations [14], the near-field excitation method [15], and highly focused optical beams [16]. However, more or less destructive interference exists in those methods, which arises from local wavevector mismatching between the spatial components of incident light and SPPs, and leads to only parts of incident light energy being able to be used and thus decreases the efficiency of SPP excitation. Hence, how to make full use of the energy of the incident light as much as possible and enhance the SPP excitation becomes more and more important in areas of the interaction between SPPs and other physical processes. There are two main methods that can be used to solve this problem. One is by carefully designing the local structure of the grating to satisfy such a full wavevector matching condition [17]. Nevertheless, this method needs precise fabrication of such structure, which challenges the fabrication technique. Another method is by controlling the incident light. Ruan *et al.* have theoretically demonstrated that the SPP field intensity can be enhanced by tailoring the illumination beam [18].

As far as we know, this is the first time to experimentally demonstrate the enhancement of SPP excitation via a feedback-based wavefront shaping method. For simplicity and without loss of generality, the Kretschmann configuration is used in our experiments. A stepwise sequential algorithm is used to search for the most optimal condition that reaches

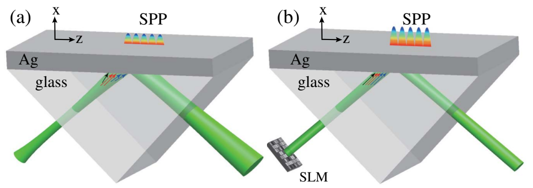

Fig. 1. Concept of the enhancement of SPP excitation via feedback-based wavefront shaping. (a) Without wavefront shaping, the incident laser beam is divergent even with the fundamental mode Gaussian beam, which results in local wavevector mismatching even if the laser is incident at the resonance angle, and which limits the SPP excitation. (b) With proper wavefront shaping by using the SLM, the local wavevector matching can be realized and the intensity of the SPP can be enhanced through constructive interference.

the maximum value of SPP intensity. After optimizing the phase profile of the incident beam at the resonance angle, the intensity is enhanced by a factor of 1.58 times. The enhancements of such SPP excitation are also analyzed when the beam is incident along an off-resonance angle and in a noisy environment.

The concept of the enhancement of SPP excitation in the Kretschmann configuration via feedback-based wavefront shaping can be illustrated in Fig. 1. A conventional TM-polarized Gaussian beam is incident onto the interface of the prism and thin silver film. The resonance will take place when changing the incident angle until the in-plane component of the incident wavevector $k_{\parallel} = k_0 n_p \sin\theta$ is equal to the wavevector of SPP $k_{\mathrm{spp}} = k_0\sqrt{\varepsilon_{rm}\varepsilon_d/(\varepsilon_{rm}+\varepsilon_d)}$, where n_p is the refractive index of prism, θ is the incident angle on the prism/metal interface, k_0 is the wavevector of incident light in vacuum, ε_{rm} is the real part of the dielectric constant of the metal, and ε_d is the refractive index of air. Without wavefront shaping, the incident beam output from the laser is divergent because of the inevitable diffraction even for the fundamental mode Gaussian beam, which results in local wavevector mismatching even when the laser is incident at the resonance angle, as illustrated in Fig. 1(a). The destructive interference will happen in the place where the wavevector components $k_{\parallel} > k_{\mathrm{spp}}$ and $k_{\parallel} < k_{\mathrm{spp}}$, and it decreases the efficiency of SPP excitation. When the phase of the incident beam is properly shaped by using a spatial light modulator (SLM), the local wavevector matching can be realized, thereby leading to a constructive interference of SPP, as illustrated in Fig. 1(b). According to the spatial coupled-mode theory (CMT), the excitation process can be written as the following expression [18]:

$$\frac{da}{dz} = (i\beta_{\mathrm{SPP}} - \alpha_l - \alpha_{\mathrm{SPP}})a + ie^{i\varphi}\sqrt{2\alpha_l}S_{in}(z), \tag{1}$$

where a is the amplitude of the SPP. S_{in} is the complex amplitude of the incident beam. φ is the phase change of the reflection at the prism/metal interface. β_{SPP} is the propagation constant of the SPP mode. α_l and α_{SPP}, respectively, correspond to the loss rate of the SPP due to the leaky radiation and the propagation loss. Note that the spatial CMT takes the approximation of the strong confinement condition, that is, $\alpha_l + |\alpha_{\mathrm{SPP}}| \ll \beta_{\mathrm{SPP}}$ [19]. Equation (1) indicates that the amplitude of the excited SPP relates to the phase and amplitude of the incident beam.

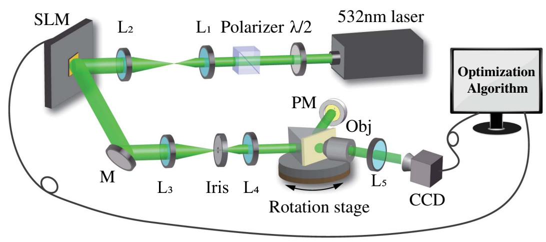

Fig. 2. Experimental setup for manipulating SPP excitation via feedback-based wavefront shaping. $\lambda/2$, half-wave plate; SLM, spatial light modulator; L_{1-5}: lens, $f_{1-5} = 50$, 200, 200, 50, and 30 mm, respectively; M, mirror; PM, power meter.

The experimental setup for manipulating SPP excitation via feedback-based wavefront shaping is depicted in Fig. 2. The 532 nm laser is used as the pump source. A half-wave plate and a Glan–Taylor polarizer are used to control the power and polarization state of the incident light. The incident light is expanded by a 4-f system, which is combined by two lenses (L_1 and L_2, of which the focal length is, respectively, 50 and 200 mm), to fill the SLM active segments as much as possible. The SLM has a resolution of 512 × 512 pixels, each with a rectangular area of 19.5 μm × 19.5 μm. After modulating through the SLM, another 4-f system consisting of L_3 and L_4 is used to shrink the waist of the laser beam and increase the modulation depth. After that, the phase modulated beam is incident onto the interface of prism/metal. In our experiments, the silver film is coated on an equilateral triangular prism ($\varepsilon = 3.24$), which is sputter-deposited in vacuum (SPF-210B, Anelva Corporation). The thickness of silver film is about 50 nm and the dielectric constant $\varepsilon_{\mathrm{Ag}} = -11.398 + 0.452i$ [20]. The prism can be rotated by a PC-controlled $\theta/2\theta$ goniometer to tune the incident angle. Finally, the scattered SPP induced light is captured by an imaging system, which consists of an objective lens (10×, NA = 0.25. 160/0.17), L_5, and a multispectral two-channel charge-coupled device (CCD) camera (MER-130-30GM). The CCD camera has a resolution of 1280 × 1024 pixels, each with a square area of 5.2 μm × 5.2 μm. The intensity of the scattering light is served as a feedback signal in the searching algorithm to enhance SPP excitation. In addition, the reflected beam is monitored by an optical power and energy meter (PM100D, Thorlabs).

SPP is strongly confined on the interface, and it is impossible to directly visualize its intensity in the far field because of its evanescent property. In previous researches, different detection techniques have been proposed, including near-field microscopy [21], fluorescence imaging [22], leakage radiation microscope [23], and scattered light imaging [24,25]. In our experiments, the scattering signal of SPP arising from the imperfection of the metal surface is used to characterize the intensity of SPP. The atomic force microscope (AFM) image of the metal surface is shown in the inset of Fig. 3(a). The surface roughness is about 80 nm. First of all, the relation between the intensity of the scattering signal and the resonance condition of the SPP is demonstrated. Figure 3(a) shows the normalized reflection intensity in the attenuation total reflection (ATR) spectrum as the function of the incident angle in the Kretschmann configuration. The experimental observation (red solid line) is in good agreement with the theoretical

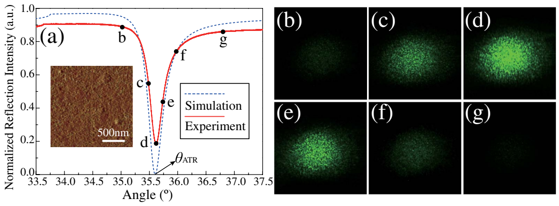

Fig. 3. (a) Normalized reflection intensity in the ATR spectrum of the Kretschmann configuration as a function of the incident angle. θ_{ATR} is the simulated value of the resonance angle. An AFM image of the silver surface is shown in the inset. (b)–(g) Intensity variations of SPP scattered patterns corresponding to six different position (from point b to point g) on the ATR spectrum.

prediction (blue dashed line). The experimental value and the theoretical prediction of the resonance angles θ_{ATR} is, respectively, 35.60° and 35.62°. The slight deviation comes from the imperfection of the actual experimental condition, such as without considering the profile of the incident beam, the actual dielectric constant of silver, and the actual thickness of the silver film used in the experiment. Figures 3(b)–3(g) present the intensity variations of SPP scattered patterns corresponding to six different positions from point b to point g on the ATR spectra of Fig. 3(a). Before reaching the resonance angle (point d), it is clear to see that the reflection intensity is continually decreasing with the increasing of the incident angle, while the scattering intensity of SPP corresponding to Figs. 3(b)–3(d) first continually increases and then reaches the maximum value. After that, the scattering intensity of SPP becomes weaker as the incident angle increases because of being far away from the wavevector matching condition, as illustrated in Figs. 3(e)–3(g). It is easy to understand that a stronger SPP field leads to stronger scattered light and weaker reflected light. Therefore, such a scattering signal of SPP can be used to characterize the intensity of SPP.

Next, a stepwise sequential algorithm is applied to search for the maximum value of the SPP intensity by optimizing the phase mask of the SLM to reshape the wavefront of the incident beam in our experiment. The optimization results are shown in Fig. 4 when a fundamental mode Gaussian beam output from a continuous-wave (CW) laser with the wavelength of 532 nm is incident onto the prism/metal interface along resonance angle $\theta_{ATR} = 35.62°$. In this algorithm, 512 × 512 pixels of the SLM are divided into 32 × 32 pixel segments to shape the wavefront of the beam. Each iteration of the algorithm optimizes one segment. The phase retardation is set to have a value between 0 and 2π in eight steps for each of the segments individually. This process is repeated four times, and the results are averaged to reduce the noise. Then the eight results are ranked according to the scattered intensity of the SPP. The phase of each segment corresponding to the maximum output intensity is recorded and stored as the optimal phase. Only after all segments are performed are the final completed optimal phase masks loaded onto the SLM. Eventually, the maximum scattering intensity of the SPP can be obtained, and its pattern can be captured by CCD. It is worth mentioning that the phase-shaped beam has the same incident power, 2.25 mW, as the initial incident Gaussian beam. The scattered intensity of the SPP is detected before and after optimization. In order to avoid the occurrence of accidental results, 200 results are continuously measured. As shown in Fig. 4(a), the scattered intensity of SPP without wavefront shaping is normalized to 1.0 (black line). It is clear to see that the intensity can be enhanced by an enhancement factor of $\eta \approx 1.58$ after wavefront shaping (red line). Figures 4(b) and 4(c) present the scattered patterns of the SPP before and after the optimization process, respectively. It is obvious that the intensity shown in Fig. 4(c) is much higher than that in Fig. 4(b). In Fig. 4(d), points A and B correspond to the reflection intensity before and after wavefront shaping, respectively. After such an optimization process, the minimum value of the reflection intensity at the resonance point decreases from 0.185 to 0.120 mW (about 35%). This indicates that more energy from incident light is transferred to the SPP. The final optimized phase mask profile is shown in Fig. 4(e).

Further, we investigate the situation of SPP excitation when the beam is incident along the off-resonance angle. As shown in Fig. 4(d), the incident angle of the beam is set at point C ($\theta = 35.72°$) before the optimization process, and the reflection intensity is 0.389 mW. After optimization by using a stepwise sequential algorithm, the reflection intensity reduces to 0.145 mW (point D, about 63%), and the final optimal phase mask is presented in Fig. 4(f). The intensity variations under off-resonance conditions before and after wavefront shaping are shown in Fig. 5(a). The left and right insets present the scattered patterns of SPP before and after optimization, respectively. The comparison of the enhancement factors η in two cases is shown in Fig. 5(b). When the beam diverges from the resonance angle, η is estimated to be 1.76 according to

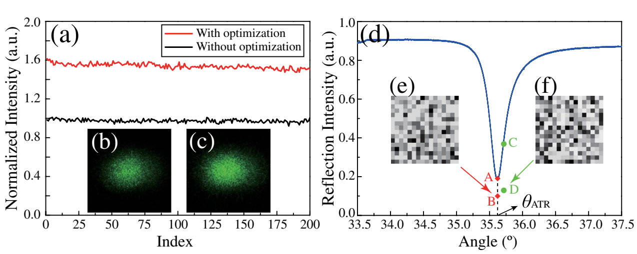

Fig. 4. Results of optimization experiment when the 532 nm CW laser is incident at the resonance angle. (a) Normalized SPP scattered intensity before (black lines) and after (red lines) the wavefront shaping process. (b) and (c) present the scattered patterns of SPP before and after optimization, respectively. (d) Reflection intensity in the ATR spectrum. (e) and (f) show the optimized phase masks after optimization at resonance and off-resonance angles, respectively.

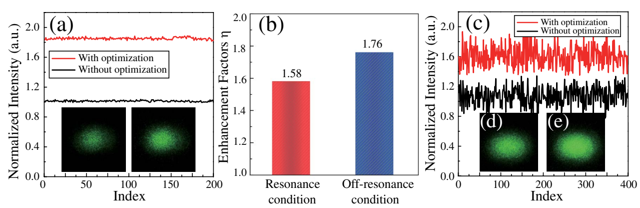

Fig. 5. (a) Results of optimization experiment of 532 nm CW laser incident at off-resonance angle. The left and right insets present the scattered patterns of SPP before and after optimization, respectively. (b) Comparison of the enhancement factors η when the beam is incident along the resonance angle and off-resonance angle. (c) Optimized results of 532 nm pulsed laser with relative higher fluctuation of the intensity. The enhancement factor is $\eta \approx 1.48$. (d) and (e) show the scattered patterns of SPP excited with initial and modulated beams, respectively.

the intensity variations in Fig. 5(a). It is larger than the case at the resonance condition $\eta \approx 1.58$. That is because the destructive interference caused by the wavevector mismatching is more apparent when rotating the prism to diverge from the resonance angle. Thus, more wavevector component can be reshaped by wavefront shaping method and finally lead to the higher enhancement factor. However, this method would be invalid for the enhancement of SPP excitation if the diverging angle is too large, which beyond the modulation limitation of the SLM. The modulation range is closely related to the phase difference and the size of neighbor phase mask segments on the SLM. In our experiments, the modulation limitation of the angle can be estimated as about $\pm 0.39°$.

In addition, to illustrate its ability in a noisy environment, a pulsed laser with relative higher fluctuation of the intensity with respect to the CW laser is used to excite SPP in our experiments. A high-energy diode-pumped all-solid-state Q-switched laser (with noise at 30% of average intensity) at the wavelength of 532 nm (10 ns) with 1 kHz repetition rate is used as the pump source, and the other experimental conditions arekept unchanged. The results are shown in Fig. 5(c), where the intensity of the enhanced scattering spot is approximately 1.48 times greater than that of the average spot intensity without optimization. Figures 5(d) and 5(e), respectively, correspond to the black and red line, and we can see that SPP scattering spot after the wavefront shaping process is much brighter than the initial spot. The optimization process is still valid in this situation. That is because the optimization loops are designed to repeat multiple times, and the results are averaged to reduce the influence of the unstable property of the pulse laser as much as possible.

In other schemes of SPP excitation, especially the case in a high numerical aperture microscope, the enhancement factor would much higher by using the method proposed here. Besides, we can expect that the enhancement factor would also be much higher when using a high-order mode of laser to excite SPPs because of the larger divergence angle. On the other hand, there are still some limitations of this method, including the optimization speed and modulation range. In our experiments, it took about 30 min to complete the optimization process. These problems are believed to be solved with a more optimized algorithm and better software–hardware configuration in the future [26].

In conclusion, as far as we know, this is the first time to experimentally demonstrate the enhancement of SPP excitation via a feedback-based wavefront shaping method. The scattering signal of an SPP is used to characterize the SPP, and the stepwise sequential algorithm is applied to search for the optimal results. After optimizing the phase profile of the incident CW laser beam at the resonance angle, the intensity of the SPP is enhanced, and the enhancement factor is about 1.58. The enhancement of SPP excitation when the beam is incident at an off-resonance angle is also analyzed, and the enhancement factor is higher than the case at the resonance angle within the scope of the modulation capacity of the SLM. In addition, the enhancements of such SPP excitation in noisy environment are also demonstrated. This work provides a flexible and convenient method to further enhance the SPP excitation and can be used to further enhance the interaction between SPPs and other physical processes.

Funding. National Key R&D Program of China (2017YFA0303700, 2018YFA0306300); National Natural Science Foundation of China (NSFC) (11734011); The Foundation for Development of Science and Technology of Shanghai (17JC1400400).

REFERENCES

1. S. A. Maier, *Plasmonics: Fundamentals and Applications* (Springer, 2007).
2. J. Homola, Chem. Rev. **108**, 462 (2008).
3. A. Bouhelier, M. Beversluis, A. Hartschuh, and L. Novotny, Phys. Rev. Lett. **90**, 013903 (2003).
4. E. M. Kim, S. S. Elovikov, T. V. Murzina, A. A. Nikulin, O. A. Aktsipetrov, M. A. Bader, and G. Marowsky, Phys. Rev. Lett. **95**, 227402 (2005).
5. J. Renger, R. Quidant, N. van Hulst, and L. Novotny, Phys. Rev. Lett. **104**, 046803 (2010).
6. Y. Liu, S. P. Xu, X. Y. Xuan, B. Zhao, and W. Q. Xu, J. Phys. Chem. Lett. **2**, 2218 (2011).
7. B. Sharma, R. R. Frontiera, A. I. Henry, E. Ringe, and R. P. Van Duyne, Mater. Today **15**(1–2), 16 (2012).
8. M. Righini, G. Volpe, C. Girard, D. Petrov, and R. Quidant, Phys. Rev. Lett. **100**, 186804 (2008).
9. N. Kinsey, M. Ferrera, V. M. Shalaev, and A. Boltasseva, J. Opt. Soc. Am. B **32**, 121 (2015).
10. N. Rahbany, W. Geng, R. Salas-Montiel, S. de la Cruz, E. R. Méndez, S. Blaize, R. Bachelot, and C. Couteau, Plasmonics **11**, 175 (2016).
11. J. Lin, J. P. B. Mueller, Q. Wang, G. H. Yuan, N. Antoniou, X. C. Yuan, and F. Capasso, Science **340**, 331 (2013).
12. R. H. Ritchie, E. T. Arakawa, J. J. Cowan, and R. N. Hamm, Phys. Rev. Lett. **21**, 1530 (1968).
13. A. Otto, Z. Phys. **216**, 398 (1968).
14. E. Kretschmann and H. Raether, Z. Naturforsch. **23**, 2135 (1968).
15. B. Hecht, H. Bielefeldt, L. Novotny, Y. Inouye, and D. W. Pohl, Phys. Rev. Lett. **77**, 1889 (1996).
16. A. Bouhelier and G. P. Wiederrecht, Phys. Rev. B **71**, 195406 (2005).
17. R. Mehfuz, M. W. Maqsood, and K. J. Chau, Opt. Express **18**, 18206 (2010).
18. Z. C. Ruan, H. Wu, M. Qiu, and S. H. Fan, Opt. Lett. **39**, 3587 (2014).
19. H. Haus, *Waves and Fields in Optoelectronics* (Prentice-Hall, 1984).
20. A. Ciesielski, L. Skowronski, M. Trzcinski, and T. Szoplik, Appl. Surf. Sci. **421**, 349 (2017).
21. J. C. Weeber, J. R. Krenn, A. Dereux, B. Lamprecht, Y. Lacroute, and J. P. Goudonnet, Phys. Rev. B **64**, 045411 (2001).
22. H. Ditlbacher, J. R. Krenn, N. Felidj, B. Lamprecht, G. Schider, M. Salerno, A. Leitner, and F. R. Aussenegg, Appl. Phys. Lett. **80**, 404 (2002).
23. A. Drezet, A. Hohenau, D. Koller, A. Stepanov, H. Ditlbacher, B. Steinberger, F. R. Aussenegg, A. Leitner, and J. R. Krenn, Mater. Sci. Eng. B **149**, 220 (2008).
24. A. V. Zayats, I. I. Smolyaninov, and A. A. Maradudin, Phys. Rep. **408**, 131 (2005).
25. L. P. Du, D. Y. Tang, and X. C. Yuan, Appl. Phys. Lett. **103**, 181101 (2013).
26. Y. Q. Qiao, Y. J. Peng, Y. L. Zheng, F. W. Ye, and X. F. Chen, Opt. Lett. **42**, 1895 (2017).